ARTICLE

A Reflectron Time-of-Flight Mass Spectrometer with a Nano-Electrospray Ionization Source for Study of Metal Cluster Compounds

Xiao-hu Wu[a], Hua Xie[a], Zhi-ling Liu[b], Hai-feng Su[c], Shui-chao Lin[c*], Zi-chao Tang[a,c*]

a. State Key Laboratory of Molecular Reaction Dynamics, Dalian Institute of Chemical Physics, Chinese Academy of Sciences, Dalian 116023, China
b. School of Chemistry & Material Science, Shanxi Normal University, Linfen 041004, China
c. State Key Laboratory for Physical Chemistry of Solid Surfaces, Collaborative Innovation Center of Chemistry for Energy Materials, and Department of Chemistry, College of Chemistry and Chemical Engineering, Xiamen University, Xiamen 361005, China

(Dated: Received on January 26, 2016; Accepted on March 1, 2016)

An experiment facility has been set up for the study of metal cluster compounds in our laboratory, which consists of a nano-electrospray ionization source, an ion transmission and focus system, and a reflectron time-of-flight mass spectrometer. Taking advantage of the nano-electrospray ionization source, polyvalent ions are usually produced in the "ionization" process and the obtained mass resolution of the equipment is over 8000. The molecular ion peaks of metal cluster compounds $[Au_{20}(PPhpy_2)_{10}Cl_2](SbF_6)_4$, where $PPhpy_2$=bis(2-pyridyl)phenylphosphine, and $[Au_6Ag_2(C)L_6](BF_4)_4$, where L=2-(diphenylphosphino)-5-methylpyridine, are distinguished in the respective mass spectrum, accompanied by some fragment ion peaks. In addition, the mass-to-charge ratios of the parent ions are determinated. Preliminary results suggest that the device is a powerful tool for the study of metal cluster compounds. It turns out that the information obtained by the instrumentation serves as an essential supplement to single crystal X-ray diffraction for structure characterization of metal cluster compounds.

Key words: Nano-electrospray ionization source, Ion transmission and focus system, Reflectron time-of-flight mass spectrometer, Metal cluster compounds, Single crystal X-ray diffraction

I. INTRODUCTION

Due to many kinds of potential applications in luminescent materials [1, 2], biology [3, 4], catalysis [5], biomedicine [6], renewable energy [7], and chemical sensing [8], metal cluster compounds, especially ligand-protected gold nanoclusters, have attracted intense research interest in recent decades [9−13]. To date, a good deal of metal cluster compounds have been prepared. The structure characterization of metal cluster compounds mostly relies on single crystal X-ray diffraction (XRD), which, however, is difficult to definitely distinguish the atoms bearing the similar number of electron (such as mercury and gold atoms [14]). Thus, determining the atomic species often needs to be inferred from the reactants and some chemical knowledge. However, in many cases, the speculation lacks of sufficient convince. On the other hand, with the development of metal cluster compounds chemistry, the study involved no longer confines to the characterization of synthetic products, also contains the characterization of the intermediate products in the synthetic reaction and the determination of the course and mechanism of the synthetic reaction. For the latter, nevertheless, it is beyond the ability of XRD. In order to solve the above problems, mass spectrometry (MS) has been introduced and promoted. In fact, MS has been the staple method to determine the identity of metal cluster compounds so far [15−17]. Compared with XRD, MS can definitely and inerrably confirm the mass-to-charge ratio of the observed ions. In many cases, MS has become an important supplement to XRD for the structure characterization of metal cluster compounds [18].

Metal cluster compounds are composed of relatively weak coordination bond between the metal core and the ligands, so they can be easily dissociated in the ionization process. As a result, the required molecular ion peaks can't be obtained in the mass spectra (or not enough outstanding). To really implement the MS analysis of metal cluster compounds, the mass spectrometer must satisfy three conditions at the same time: firstly, the ion source must be "soft", like electrospray ionization (ESI) source [19−21]; secondly, ion transport and focus system must be also "moderate", en-

*Authors to whom correspondence should be addressed. E-mail: zctang@dicp.ac.cn, sclin@xmu.edu.cn, Tel.: +86-411-84379365, +86-592-2183047, FAX: +86-411-84675584, +86-592-2183047.

suring the ions stability in the transmission process; lastly, the mass analyzer must have very wide mass detection range and high resolution. In addition, the metal parts of metal cluster compounds can easily deposite within the mass spectrometer in the analysis process, causing signal contamination and performance reduction of the instrument. Based on the aforementioned considerations, an experiment facility has been constructed for the study of metal cluster compounds in our laboratory, which includes a nano-electrospray ionization (nano-ESI) source [22, 23], an ion transmission and focus system and a reflectron time-of-flight mass spectrometer (ReTOFMS) [24]. In the current work, we will introduce this setup in detail, and some preliminary results with respect to metal cluster compounds $[Au_{20}(PPhpy_2)_{10}Cl_2](SbF_6)_4$ ($PPhpy_2$=bis(2-pyridyl)phenylphosphine) and $[Au_6Ag_2(C)L_6](BF_4)_4$ (L=2-(diphenylphosphino)-5-methylpyridine) are presented, as well as the relevant results and conclusions.

II. EXPERIMENTAL APPARATUS

The experiment setup, which includes a nano-ESI source, an ion transmission and focus system and a ReTOFMS, is shown schematically in Fig.1. According to the vacuum condition, the instrument is divided into three regions labeled as I, II, and III in Fig.1. A stainless steel plate with an aperture diameter of 1 mm (aperture plate 1) separates region I and II, while the separation between region II and III is achieved by a stainless steel plate (aperture plate 4) with an aperture diameter of 2 mm. The pressures of region I and III, which are monitored by a resistance gauge and a ionization gauge, respectively, are ca. 110 and 1.4×10^{-4} Pa when the setup is in running mode, while they reduce to ca. 1.7 and 3.5×10^{-5} Pa as in standby mode, respectively. The vacuum of region II and III is respectively maintained by one 450 L/s turbomolecular pump and another 450 L/s turbomolecular pump, both of which are backed together by an 8 L/s mechanical pump simultaneously employed to evacuate the air in region I.

A. Ion source

The nano-ESI source used here, attributed to its low consumption of sample solution, essentially consists of a capillary spray needle, a stainless steel wire and a counter plate (herein, referred to as nozzle). The capillary spray needles, into which the analyte solution of trace volume is put by a microliter syringe, are made by pulling the borosilicate glass capillaries (0.89 mm in internal diameter, 1.2 mm in outside diameter, and 10 cm in length) with a simple home-made puller. The glass capillaries end in a very fine glass cone tip, the orifice diameter of which is 200−300 μm. The stainless steel wire (0.5 mm in diameter) is placed in the spray capillary for the connection to the power supply. The voltage applied to the spray needle is in the range of 1600−2000 V, much lower compared with that in the ESI source (usually 3000−4000 V). The nozzle with an orifice diameter of 0.5 mm is also adopted to accomplish a differential vacuum between the surrounding atmosphere environment and region I. Compared to the ESI source and according to the obtained results below, the desolvation efficiency of the current source is high enough for the analysis of sample solution of metal cluster compounds. Therefore, a nitrogen gas curtain between the spray needle and the nozzle is not used here. In order to avoid a large amount of analyte solution entering and polluting the setup, the orifice of the capillary spray needle is placed slightly above that of the nozzle rather than opposite directly to the nozzle orifice.

B. Ion transmission and focus system

After travelling through the nozzle orifice, the analyte ions produced by the atmospheric nano-ESI source enter an ion transmission and focus system, which chiefly comprises two different RF-only hexapoles (hexapole 1 and hexapole 2, as shown in Fig.1), a RF-only quadrupole and an einzel lens. The typical operation parameters of the system include nozzle potential of 91.0 V, hexapole 1 bias of 59.6 V, aperture plate 1 potential of 6.88 V, hexapole 2 bias of 5.85 V, hexapole RF amplitude of 300 V (zero-to-peak), hexapole frequency of 690 kHz, aperture plate 2 potential of 4.16 V, quadrupole bias of 2.98 V, quadrupole RF amplitude of 300−1000 V (zero-to-peak), quadrupole frequency of 720 kHz, aperture plate 3 potential of −29.4 V, einzel lens-up of 4.29 V, einzel lens-down of 3.95 V, aperture plate 4 potential and slit potential being grounded.

Hexapole 1, mainly acting as desolvation effect, is made of six cylindrically shaped stainless steel rod electrodes. Different from hexapole 1, hexapole 2, composed of six cylindrically shaped stainless steel rod electrodes, primarily plays a guiding role, despite that desolvation perhaps takes place therein. The amplitude and frequency of RF voltage applied to hexapole 2 are identical with that applied to hexapole 1. Four cylindrically shaped stainless steel rod electrodes constitute the quadrupole which plays a guiding role as well, although the quadrupole has the mass-selective function, however, which is not explored in the present instrument. Due to the mass discrimination effect of the quadrupole, the ions (m/z<ca.350) will be lost when passing through the quadrupole and thus can't be detected on the MCP. The amplitude of RF voltage applied to the quadrupole is variable dependent on the mass detection range set while the frequency of that is constant. It is worth noting that the length and diameter of the cylindrically shaped stainless steel rod electrodes in hexapole 1, hexapole 2, and the quadrupole are not identical with each other, respectively. At last,

DOI:10.1063/1674-0068/29/cjcp1601019

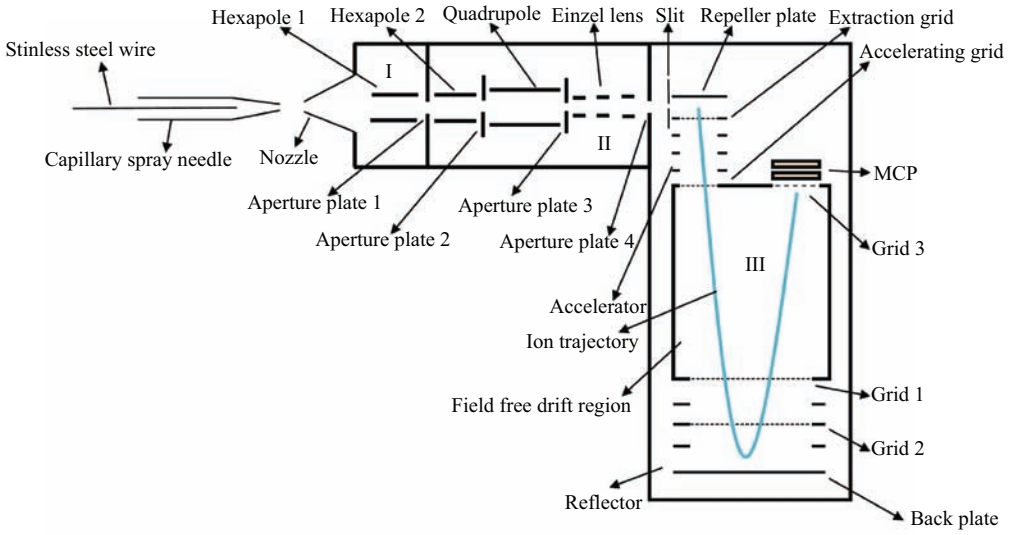

FIG. 1 Schematic diagram of the experiment setup containing a nano-electrospray ionization source, an ion transmission and focus system and a reflectron time-of-flight mass spectrometer.

after transporting through the two hexapoles and the quadrupole, the ion beam, which becomes focused and cooled, is then converted into the parallel one while passing the einzel lens. In order to improve the ion transport efficiency, different potentials are exerted on the elements to form a successive longitudinal electric field. As a result, the ion transport efficiency of metal cluster compounds is about 0.1% by using the picoammeter to measure the electric current. In detail, the ions mostly loss in three places (nozzle, aperture plate 1, and aperture plate 4), that is, when going through each differential vacuum aperture, the ions will loss ca. 90%.

C. ReTOFMS

After going through the ion transmission and focus system, aperture plate 4 and a slit, the analyte ions from the parallel beam are transmitted into a ReTOFMS. The typical operation parameters of ReTOFMS include repeller plate pulse magnitude of +1000 V (3 kHz), extraction grid pulse magnitude of −1000 V (3 kHz), acceleration grid potential of −4059 V, grid 1 potential of −4059 V, grid 2 potential of 189 V, back plate potential of 1002.5 V, grid 3 potential of −4059 V, and MCP voltage of 1700 V. The ReTOFMS prevailingly embodies an accelerator, a field free drift region, and a reflector. All data in the present work are collected in positive ion mode. The positive ions are immediately accelerated into the mass analyzer as soon as the positive and negative pulse voltages are simultaneously applied to the repeller plate and extraction grid, respectively, and then detected by the MCP. In order to prevent the analyte cations diffusing toward the extraction grid before the positive and negative pulse voltages are applied, resulting in the reduction of the mass resolution, a positive offset voltage (5−10 V) is applied to the negative pulse voltages in series. All voltages of the instrument are supplied by the house-built integrated circuit controlled by the computer. The mass spectra are recorded by an analog-to-digital converter acquisition card (2 GHz) and the acquisition frequency is set at 3 kHz.

III. PRELIMINARY RESULTS AND DISCUSSIONS

Metal cluster compounds $[Au_6Ag_2(C)L_6](BF_4)_4$ and $[Au_{20}(PPhpy_2)_{10}Cl_2](SbF_6)_4$ were provided by Quanming Wang group in Xiamen University. Their synthetic methods and structures of were referred to literatures [25] and [26], respectively. The solvents methanol (CH_3OH, AR grade) and acetonitrile (CH_3CN, AR grade) employed were commercially available and used as received. Stock solutions of two compounds were prepared in CH_3OH and CH_3CN, respectively, at a concentration 1 mg/mL. Diluted solutions, which were prepared from the stock solutions, both diluted 1:10 with CH_3OH, were introduced directly into the spectrometer. All peaks in the mass spectra were identified by the most intense peak in the isotopic mass distribution.

A. $[Au_{20}(PPhpy_2)_{10}Cl_2](SbF_6)_4$

Figure 2 shows the mass spectrum of $[Au_{20}(PPhpy_2)_{10}Cl_2](SbF_6)_4$ dissolved in methanol solvent. Figure 3 presents the expansion of the isotope peak (m/z=725.13) corresponding to $\{Au(PPhpy_2)_2\}^{2+}$ ion in the mass spectrum of $[Au_{20}(PPhpy_2)_{10}Cl_2](SbF_6)_4$. The mass resolution R is about 8240 (over 8000) for m/z=725.13 isotope peak in Fig.3. Five peaks are assigned by their

DOI:10.1063/1674-0068/29/cjcp1601019

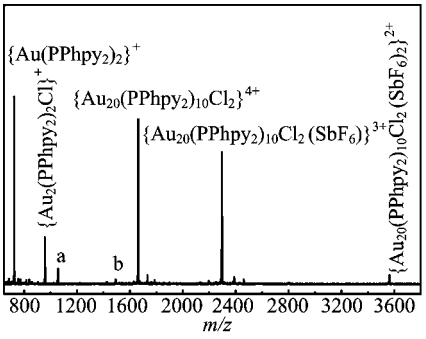

FIG. 2 The mass spectrum of $[Au_{20}(PPhpy_2)_{10}Cl_2](SbF_6)_4$ dissolved in methanol solvent. a: $\{Au_2Cu(PPhpy_2)_2Cl_2\}^{2+}$, b: $\{Au_{11}Cu_2(PPhpy_2)_8Cl_2\}^{3+}$.

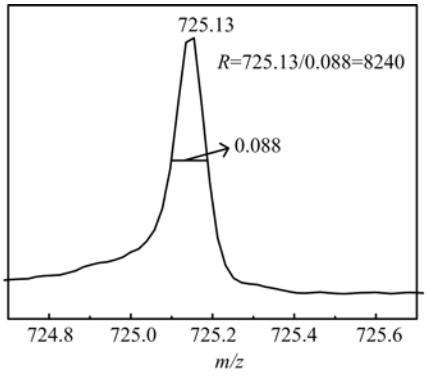

FIG. 3 The expansion of the isotope peak (m/z=725.13) corresponding to $\{Au(PPhpy_2)_2\}^{2+}$ ion in the mass spectrum of $[Au_{20}(PPhpy_2)_{10}Cl_2](SbF_6)_4$.

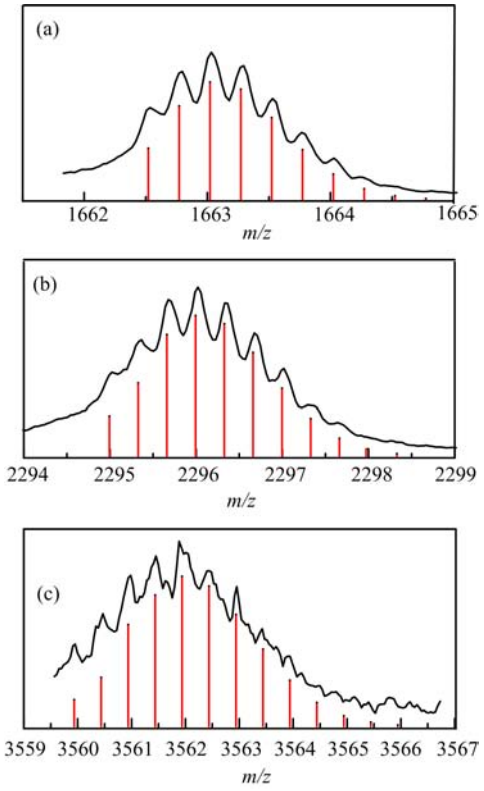

FIG. 4 The experimental measured (black trace) and theoretical simulated (red vertical bar) isotopic patterns of (a) $\{Au_{20}(PPhpy_2)_{10}Cl_2\}^{4+}$, (b) $\{Au_{20}(PPhpy_2)_{10}Cl_2(SbF_6)\}^{3+}$ and (c) $\{Au_{20}(PPhpy_2)_{10}Cl_2(SbF_6)_2\}^{2+}$.

mass-to-charge ratios as indicated in Fig.2. Although the most intense peak at m/z=725.13 corresponds to the fragment ion $\{Au(PPhpy_2)_2\}^+$, and the much weaker peak at m/z=957.05 is assigned to the fragment ion $\{Au_2(PPhpy_2)_2Cl\}^+$, the molecular ion peak at m/z=1662.97, corresponding to the tetravalent cation $\{Au_{20}(PPhpy_2)_{10}Cl_2\}^{4+}$, is comparatively prominent. Moreover, compared with the molecular ion peak, the minor peaks at m/z=2296.02 and 3562.08, which are attributed to $\{Au_{20}(PPhpy_2)_{10}Cl_2(SbF_6)\}^{3+}$ and $\{Au_{20}(PPhpy_2)_{10}Cl_2(SbF_6)_2\}^{2+}$ derived from the binding of one counter anion and two counter anions, respectively, to $\{Au_{20}(PPhpy_2)_{10}Cl_2\}^{4+}$, are also observed.

The measured isotopic patterns of $\{Au_{20}(PPhpy_2)_{10}Cl_2\}^{4+}$ and $\{Au_{20}(PPhpy_2)_{10}Cl_2(SbF_6)\}^{3+}$ are faultlessly consistent with the theoretical simulated ones, as shown in Fig.4 (a) and (b), respectively, while the experimental measured isotopic pattern of $\{Au_{20}(PPhpy_2)_{10}Cl_2(SbF_6)_2\}^{2+}$ is intangibly in accordance with the theoretical simulated one (Fig.4(c)), owing to the fairly weak intensity. In addition, two peaks labeled as a (m/z=1056.95) and b (m/z=1492.65) are assigned to the fragment ions $\{Au_2Cu(PPhpy_2)_2Cl_2\}^+$ and $\{Au_{11}Cu_2(PPhpy_2)_8Cl_2\}^{3+}$, respectively. The two peaks are probably derived from the pollutant $[Au_{13}Cu_2(dppy)_8Cl_4](BF_4)_3$ (dppy=bisphenyl-2-pyridylphosphine), because they are not observed in the spectrum (as shown in Fig.5) before the analyte $[Au_{13}Cu_2(dppy)_8Cl_4](BF_4)_3$ are sampled. The above mentioned observations and results further confirm that: firstly, the counter ion is SbF_6^- because of the presence of $\{Au_{20}(PPhpy_2)_{10}Cl_2(SbF_6)\}^{3+}$ and $\{Au_{20}(PPhpy_2)_{10}Cl_2(SbF_6)_2\}^{2+}$; secondly, the maximum number of the counter ions is four due to the absence of $\{Au_{20}(PPhpy_2)_{10}Cl_2\}^{5+}$, $\{Au_{20}(PPhpy_2)_{10}Cl_2\}^{6+}$ *etc.*; lastly, the composition is $[Au_{20}(PPhpy_2)_{10}Cl_2](SbF_6)_4$ owing to the presence of molecular ion $\{Au_{20}(PPhpy_2)_{10}Cl_2\}^{4+}$. Hence, the results obtained by MS are perfectly in agreement with that of XRD structural analysis.

Furthermore, it is concluded that the chloride and phosphine ligands in $\{Au_{20}(PPhpy_2)_{10}Cl_2\}^{4+}$ are intensely bound to the Au_{20} core with the core retaining intact, unlike that in $[Au_{20}(PPhpy_2)_{10}Cl_4]Cl_2$ [25], because we don't observe the fragment ions coming from the removal of chloride or phosphine ligands from $\{Au_{20}(PPhpy_2)_{10}Cl_2\}^{4+}$. Meanwhile, $\{Au_{20}(PPhpy_2)_{10}Cl_2\}^{4+}$ is reasonably stable, which is due to the geometrical factor similar to $[Au_{20}(PPhpy_2)_{10}Cl_4]Cl_2$ [25], because the total number

DOI:10.1063/1674-0068/29/cjcp1601019

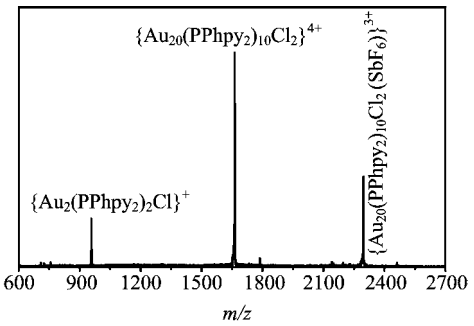

FIG. 5 The mass spectrum of $[Au_{20}(PPhpy_2)_{10}Cl_2](SbF_6)_4$ dissolved in methanol solvent before the analyte $[Au_{13}Cu_2(dppy)_8Cl_4](BF_4)_3$ are sampled.

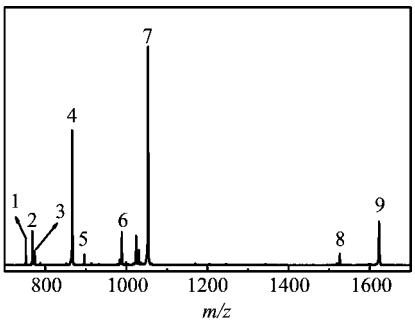

FIG. 6 The mass spectrum of $[Au_6Ag_2(C)L_6](BF_4)_4$ dissolved in CH_3CN. 1−9: $\{AuL_2\}^+$, $\{Au_6Ag_2(C)L_6\}^{4+}$, $\{Au_5Ag_2(C)L_4\}^{3+}$, $\{Au_5Ag_2(C)L_5\}^{3+}$, $\{Au_6Ag(C)L_5\}^{3+}$, $\{Au_6Ag(C)L_6\}^{3+}$, $\{Au_6Ag(C)L_6(BF_4)\}^{3+}$, $\{Au_6Ag(C)L_6(BF_4)\}^{2+}$, $\{Au_6Ag_2(C)L_6(BF_4)_2\}^{2+}$, respectively.

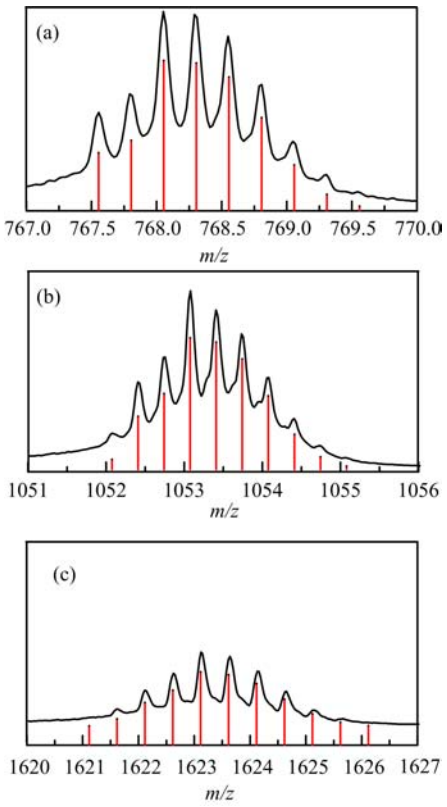

FIG. 7 The experimental measured (black trace) and theoretical simulated (red vertical bar) isotopic patterns of (a) $\{Au_6Ag_2(C)L_6\}^{4+}$, (b) $\{Au_6Ag_2(C)L_6(BF_4)\}^{3+}$, and (c) $\{Au_6Ag_2(C)L_6(BF_4)_2\}^{2+}$.

of valence electrons of $\{Au_{20}(PPhpy_2)_{10}Cl_2\}^{4+}$, calculated to be 14 ($n$=20−2−4), does not correspond to a filled spherical electronic shell of the noble gas superatom model [27], which is derived from jellium models of bare gas-phase clusters [28].

B. $[Au_6Ag_2(C)L_6](BF_4)_4$

The mass spectrum of bimetal cluster compound $[Au_6Ag_2(C)L_6](BF_4)_4$ dissolved in acetonitrile solvent is illustrated in Fig.6. Herein, nine peaks are assigned by their mass-to-charge ratios. The peak at m/z=751.20 corresponds to the fragment ion $\{AuL_2\}^+$, while the peak at m/z=768.10 is assigned to the molecular ion $\{Au_6Ag_2(C)L_6\}^{4+}$. The peaks at m/z=1053.13 and 1623.18 correspond to two counter anion BF_4^- adducts $\{Au_6Ag_2(C)L_6(BF_4)\}^{3+}$ and $\{Au_6Ag_2(C)L_6(BF_4)_2\}^{2+}$ respectively, while the peaks at m/z=988.48 and 1526.22 are assigned to $\{Au_6Ag(C)L_6\}^{3+}$ and $\{Au_6Ag(C)L_6(BF_4)\}^{2+}$ coming from the removal of a reactant $AgBF_4$ from $\{Au_6Ag_2(C)L_6(BF_4)\}^{3+}$ and $\{Au_6Ag_2(C)L_6(BF_4)_2\}^{2+}$ respectively. In addition, a weak peak (m/z=896.11), assigned to $Au_6Ag(C)L_5\}^{3+}$ is produced from $\{Au_6Ag(C)L_6\}^{3+}$ by losing one phosphine ligand. Confusingly, a fairly intense peak (m/z=866.10) and a much weaker peak (m/z=773.73), attributed to $\{Au_5Ag_2(C)L_5\}^{3+}$ and $Au_5Ag_2(C)L_4\}^{3+}$, respectively, are observed.

As shown in Fig.7, the experimental measured isotopic patterns of $\{Au_6Ag_2(C)L_6\}^{4+}$, $\{Au_6Ag_2(C)L_6(BF_4)^{3+}$ and $\{Au_6Ag_2(C)L_6(BF_4)_2\}^{2+}$ are completely in agreement with the theoretical simulated ones, respectively. Analogously, referring to $[Au_{20}(PPhpy_2)_{10}Cl_2](SbF_6)_4$, it is also further proved to be that the composition is $[Au_6Ag_2(C)L_6](BF_4)_4$ and the results obtained by MS match the results from XRD structural analysis well. Thus, MS can become an important and essential supplement to XRD for structure characterization.

Meanwhile, based on the above results of $[Au_6Ag_2(C)L_6](BF_4)_4$, it is deduced that the face-capped silver atoms [26] are weakly bonded to Au_3 triangle because of the presence of $\{Au_6Ag(C)L_6\}^{3+}$ and $\{Au_6Ag(C)L_6(BF_4)\}^{2+}$, while the phosphine ligands, when the Au_6 core, in the middle of which a carbon atom sits [26] keeps unbroken, are tightly coordinated to the core although a much weaker peak $\{Au_6Ag(C)L_5\}^{3+}$ is observed. In fact, compared with $\{Au_6Ag_2(C)L_6(BF_4)\}^{3+}$, three of the phosphine ligands

DOI:10.1063/1674-0068/29/cjcp1601019

in $\{Au_6Ag(C)L_6\}^{3+}$ are much free and unsteady when a silver atom loses, due to elimination of the bonds between the nitrogen atoms of the 5-methylpyridyl of the phosphine ligands and the silver atom. Therefore, a phosphine ligand in $\{Au_6Ag(C)L_6\}^{3+}$ maybe lose, resulting in a small amount of production of $\{Au_6Ag(C)L_5\}^{3+}$. On the other hand, the presence of $\{Au_5Ag_2(C)L_5\}^{3+}$ and $\{Au_5Ag_2(C)L_4\}^{3+}$ suggests that the interaction between the phosphine ligands and the Au_6 kernel becomes much looser, namely, the Au−P bonds turn into much weaker ones as a result of the relatively readily removal of a phosphine ligand when the Au_6 core becomes broken, herein losing one gold atom.

IV. CONCLUSION

In summary, an experiment setup constructed for the study of metal cluster compounds has been introduced. Combining with the nano-ESI source, the obtained mass resolution is over 8000. With respect to $[Au_{20}(PPhpy_2)_{10}Cl_2](SbF_6)_4$ and $[Au_6Ag_2(C)L_6](BF_4)_4$, the highly resolved mass spectra enable us to further verify their compositions obtained by the previously reported XRD structure analyses, which suggests that MS can become an important supplement to XRD for structure characterization. Moreover, the chloride and phosphine ligands in $\{Au_{20}(PPhpy_2)_{10}Cl_2\}^{4+}$ are strongly bound to the Au_{20} core protecting the core intact, while the phosphine ligands are tightly coordinated to the Au_6 core, when the cores keep unbroken. This result suggests that the interaction between the centered metal core and ligands can be estimated by MS. Taking the results together, it is considered that the device is a powerful tool for the study of metal cluster compounds.

V. ACKNOWLEDGMENTS

We thank Professor Quan-ming Wang for providing the metal cluster compounds samples. This work was supported by the National Natural Science Foundation of China (No.21103186, No.21273233, and NO.21227001), the Ministry of Science and Technology of China, and the Chinese Academy of Sciences.

[1] H. Häkkinen, Nat. Chem. **4**, 443 (2012).
[2] R. C. Jin, Y. Zhu, and H. F. Qian, Chem. Eur. J. **17**, 6584 (2011).
[3] J. P. Wilcoxon and B. L. Abrams, Chem. Soc. Rev. **35**, 1162 (2006).
[4] M. C. Daniel and D. Astruc, Chem. Rev. **104**, 293 (2004).
[5] G. Li, C. J. Zeng, and R. C. Jin, J. Am. Chem. Soc. **136**, 3673 (2014).
[6] X. D. Zhang, Z. T. Luo, J. Chen, X. Shen, S. S. Song, Y. M. Sun, S. J. Fan, F. Y. Fan, D. T. Leong, and J. P. Xie, Adv. Mater. **26**, 4565 (2014).
[7] Y. S. Chen, H. Choi, and P. V. Kamat, J. Am. Chem. Soc. **135**, 8822 (2013).
[8] Z. K. Wu, M. Wang, J. Yang, X. H. Zheng, W. P. Cai, G. W. Meng, H. F. Qian, H. M. Wang, and R. C. Jin, Small **8**, 2028 (2012).
[9] Y. Kamei, Y. Shichibu, and K. Konishi, Angew. Chem. Int. Ed. **50**, 7442 (2011).
[10] J. Chen, Q. F. Zhang, T. A. Bonaccorso, P. G. Williard, and L. S. Wang, J. Am. Chem. Soc. **136**, 92 (2013).
[11] A. Das, T. Li, K. Nobusada, C. J. Zeng, N. L. Rosi, and R. C. Jin, J. Am. Chem. Soc. **135**, 18264 (2013).
[12] H. Y. Yang, Y. Wang, J. Z. Yan, X. Chen, X. Zhang, H. Häkkinen, and N. F. Zheng, J. Am. Chem. Soc. **136**, 7197 (2014).
[13] P. Maity, S. Takano, S. Yamazoe, T. Wakabayashi, and T. Tsukuda, J. Am. Chem. Soc. **135**, 9450 (2013).
[14] K. R. Flower, R. G. Pritchard, and A. T. McGown, Angew. Chem. Int. Ed. **45**, 6535 (2006).
[15] H. F. Qian, Y. Zhu, and R. C. Jin, Proc. Natl. Acad. Sci. USA **109**, 696 (2012).
[16] Y. Negishi, Y. Takasugi, S. Sato, H. Yao, K. Kimura, and T. Tsukuda, J. Am. Chem. Soc. **126**, 6518 (2004).
[17] P. R. Nimmala and A. Dass, J. Am. Chem. Soc. **133**, 9175 (2011).
[18] H. Y. Yang, Y. Wang, J. Lei, L. Shi, X. H. Wu, V. Mäkinen, S. C. Lin, Z. C. Tang, J. He, H. Häkkinen, L. S. Zheng, and N. F. Zheng, J. Am. Chem. Soc. **135**, 9568 (2013).
[19] M. Dole, L. L. Mack, R. L. Hines, R. C. Mobley, L. D. Ferguson, and M. B. Alice, J. Chem. Phys. **49**, 2240 (1968).
[20] C. M. Whitehouse, R. N. Dreyer, M. Yamashita, and J. B. Fenn, Anal. Chem. **57**, 675 (1985).
[21] J. B. Fenn, J. Am. Soc. Mass Spectrom. **4**, 524 (1993).
[22] M. S. Wilm and M. Mann, Int. J. Mass Spectrom. Ion Proc. **136**, 167 (1994).
[23] M. Wilm and M. Mann, Anal. Chem. **68**, 1 (1996).
[24] A. N. Verentchikov, W. Ens, and K. G. Standing, Anal. Chem. **66**, 126 (1994).
[25] X. K. Wan, Z. W. Lin, and Q. M. Wang, J. Am. Chem. Soc. **134**, 14750 (2012).
[26] J. H. Jia and Q. M. Wang, J. Am. Chem. Soc. **131**, 16634 (2009).
[27] M. Walter, J. Akola, O. Lopez-Acevedo, P. D. Jadzinsky, G. Calero, C. J. Ackerson, R. L. Whetten, H. Grönbeck, and H. Häkkinen, Proc. Natl. Acad. Sci. USA **105**, 9157 (2008).
[28] W. D. Knight, K. Clemenger, W. A. de Heer, W. A. Saunders, M. Y. Chou, and M. L. Cohen, Phys. Rev. Lett. **52**, 2141 (1984).

DOI:10.1063/1674-0068/29/cjcp1601019